Published OnlineFirst August 6, 2018; DOI: 10.1158/1535-7163.MCT-18-0212

Small Molecule Therapeutics

Molecular Cancer Therapeutics

Phage Display-Derived Peptide-Based Dual-Modality Imaging Probe for Bladder Cancer Diagnosis and Resection Postinstillation: A Preclinical Study

Li Peng[1,2,3], Wenting Shang[2,4], Pengyu Guo[1,2,3], Kunshan He[2,4], Hongzhi Wang[1,3], Ziyu Han[2,4], Hongmei Jiang[2,4], Jie Tian[2,4,5], Kun Wang[2,4], and Wanhai Xu[1,3]

Abstract

Bladder cancer is a common human malignancy. Conventional ultrasound and white-light cystoscopy are often used for bladder cancer diagnosis and resection, but insufficient specificity results in a high bladder cancer recurrence rate. New strategies for the diagnosis and resection of bladder cancer are needed. In this study, we developed a highly specific peptide-based probe for bladder cancer photoacoustic imaging (PAI) diagnosis and near-infrared (NIR)-imaging-guided resection after instillation. A bladder cancer–specific peptide (PLSWT7) was selected by *in vivo* phage-display technology and labeled with IRDye800CW to synthesize a bladder cancer–specific dual-modality imaging (DMI) probe (PLSWT7-DMI). The feasibility of PLSWT7-DMI–based dual-modality PAI-NIR imaging was assessed *in vitro*, in mouse models, and *ex vivo* human bladders. An air-pouch bladder cancer (APBC) model suitable for probe instillation was established to evaluate the probe-based bladder cancer PAI diagnosis and NIR-imaging–guided resection. Human bladders were used to assess whether the PLSWT7-DMI–based DMI strategy is a translatable approach for bladder cancer detection and resection. The probe exhibited excellent selectivity and specificity both *in vitro* and *in vivo*. Postinstillation of the probe, tumors <3 mm were detectable by PAI, and NIR-imaging–guided tumor resection decreased the bladder cancer recurrence rate by 90% and increased the survival in the mouse model. Additionally, *ex vivo* NIR imaging of human bladders indicated that PLSWT7-DMI–based imaging would potentially allow precise resection of bladder cancer in clinical settings. This PLSWT7-DMI–based DMI strategy was a translatable approach for bladder cancer diagnosis and resection and could potentially lower the bladder cancer recurrence rate. *Mol Cancer Ther; 17(10); 2100–11. ©2018 AACR.*

Introduction

Bladder cancer is a common human malignancy (1). In China, the bladder cancer incidence rate is 80.5 per 100,000 individuals, and this rate is increasing (2). About 70% of patients present with non–muscle-invasive bladder cancer (NMIBC; ref. 3). Conventional ultrasound and white-light cystoscopy (WLC) are widely used for NMIBC diagnosis and resection (4, 5), but fail to prevent cancer recurrence, estimated at 15% to 61% at 1 year and 50% to 70% at 5 years (6) owing to a lack of specificity.

Despite its low accuracy in detecting small foci, conventional ultrasound has been proposed as the initial test for bladder cancer (4). Photoacoustic imaging (PAI) is an emerging technology based on ultrasound; however, unlike ultrasound, which measures only mechanical contrast, PAI measures both optical and thermo-elastic contrast (7), thereby providing better resolution and sensitivity for the early detection of small tumors. WLC, the gold standard for NMIBC diagnosis and commonly used for resection (5), has difficulty visualizing small foci and flat neoplasms as well as defining exact bladder cancer margins. Therefore, there is a high risk of leaving tumor residuals, which contribute to the high recurrence rate (8). Although hexaminolevulinate (HAL)-guided blue-light fluorescence cystoscopy enables more accurate bladder cancer detection and can reduce recurrence rates (9), its false-positive rate is high (30%) due to a low specificity (10). Therefore, better imaging agents are urgently needed to facilitate bladder cancer resection.

Molecular imaging using targeted probes is a promising approach to enhance cancer identification and guide resection (11). Among various probes, peptides have their own benefits, e.g., small size, superior specificity and selectivity, good penetration, low cost, and favorable biocompatibility (12). Phage

[1]Urology Surgery Department, The Fourth Hospital of Harbin Medical University, Harbin, Heilongjiang, P.R. China. [2]CAS Key Laboratory of Molecular Imaging, The State Key Laboratory of Management and Control for Complex Systems, Institute of Automation, Chinese Academy of Sciences, Beijing, P.R. China. [3]Heilongjiang Key Laboratory of Scientific Research in Urology, Harbin, Heilongjiang, P.R. China. [4]The State Key Laboratory of Management and Control for Complex Systems, Institute of Automation, Chinese Academy of Sciences, Beijing, China. [5]Beihang University, Beijing, P.R. China.

Note: Supplementary data for this article are available at Molecular Cancer Therapeutics Online (http://mct.aacrjournals.org/).

L. Peng, W. Shang, and P. Guo share first authorship of this article.

Corresponding Authors: Wanhai Xu, The Fourth Hospital of Harbin Medical University, Yiyuan Street #37, Nangang district, Harbin, Heilongjiang 150001, P.R. China. Phone: 86-1331-3602566; Fax: 86-0451-82576509; E-mail: xuwanhai@163.com; Jie Tian, Zhongguancun East Road #95, Haidian Dist. Beijing 100190, P. R. China. Phone: 86-10-82618465; Fax: 86-10-62527995; E-mail: jie.tian@ia.ac.cn; and Kun Wang, Zhongguancun East Road #95, Haidian Dist. Beijing 100190, P. R. China. Fax: 86-10-62527995; E-mail: Kun.wang@ia.ac.cn

doi: 10.1158/1535-7163.MCT-18-0212

Published OnlineFirst August 6, 2018; DOI: 10.1158/1535-7163.MCT-18-0212

display has been successfully used to select peptides specific for molecular signatures or biomarkers in tumor tissues (13), and tumor-targeting peptides have been labeled with fluorescein to identify cancer (14, 15). In the present work, we identified a bladder cancer cell–specific peptide by the *in vivo* screening of a phage-display peptide library, labeled the peptide with IRDye800CW NHS ester to synthesize a bladder cancer–targeted probe (PLSWT7-DMI), and evaluate its feasibility for bladder cancer management. Because the bladder is a hollow organ, probes should be administrated by instillation (intravesical administration) rather than intravenous injection. Therefore, we established a mouse air-pouch bladder cancer (APBC) model suitable for probe instillation and used this model for *in vivo* experiment. Human bladders were used to assess the potential of PLSWT7-DMI for clinical translation.

Materials and Methods

Cell culture

The human bladder cancer cell lines EJ and RT112 and human normal urothelial cell line SV-HUC-1 were obtained from the Cell Culture Center of the Institute of Basic Medical Science (Chinese Academy of Medical Sciences) in 2016. The cell lines were checked and authenticated within 6 months using STR analysis (Biowing). Cells were grown at 37°C and 5% CO_2 under a humidified atmosphere. Cells were maintained in Dulbecco's Modified Eagle's Medium (DMEM; Invitrogen Life Technology) supplemented with 10% FBS.

Establishment of a bladder cancer mouse model

BALB/c *nu*/*nu* female mice (5 weeks old) were purchased from the Vital River Laboratory Animal Technology Co. Ltd. All animal experimental protocols were approved by the Institutional Animal Care and Ethics Committee of the Fourth Hospital of Harbin Medical University, and all the methods were carried out in accordance with the approved guidelines.

Establishment of a subcutaneous mouse model

Approximately 2×10^6 RT112 tumor cells in 100 μL of DMEM were subcutaneously injected into the elbow-back region of each mouse. Visible tumors formed after ∼3 days.

Establishment of an orthotopic mouse model

Mice were anesthetized using sodium pentobarbital and catheterized with a modified IV catheter (24 G). The inner surface of the bladder was successively washed with HCl and NaOH to induce minor damage to epithelial cells. Subsequently, the inner bladder surface was washed with PBS to eliminate residual NaOH. Finally, 100 μL of RT112-luc cells (1×10^7) was infused and incubated in the bladder for 2 hours.

To confirm tumor growth in the bladder, luciferin was injected intraperitoneally into mice at a dose of 150 mg/kg body weight. Mice were then anesthetized and placed on the imaging stage of the IVIS Spectrum imaging system (Xenogen) in the abdominal position, and images were collected 10 minutes after luciferin injection.

Establishment of an APBC mouse model

Mice were anesthetized using isoflurane, and 3 mL of filtered sterile air was injected subcutaneously into their backs to create a 2.5 × 2 cm air pouch, followed by injection with 1 mL of sterile air every other day to maintain the air-pouch size. After 5 days, RT112 cells (5×10^6) in 50 μL of Matrigel were injected into the air pouch. Tumor growth was observed daily, and mice with visible tumors were selected for further experiments.

In vivo phage-display selection of tumor-targeting clones

For the selection of bladder cancer–binding phage clones, the Ph.D.-C7C Phage-display Peptide Library Kit (New England Biolabs) was used as previously described (16). Subcutaneous tumor-bearing mice received 3×10^{10} plaque-forming units (PFU) of the phage peptide library via tail-vein injection. After 15 minutes, mice were sacrificed and perfused by injection of 50 mL of PBS through the heart to wash unbound phages. Then, a portion of tumors was harvested and preserved in 4% paraformaldehyde and the rest was manually homogenized and washed with 10 × TBS containing 0.1% Tween-20 (0.1% TBST) to remove nonspecifically bound phages. Cell membrane–bound phages were eluted with 1 mL of elution buffer (0.2 mol/L glycine-HCl, pH 2.2, 1 mg/mL BSA) for 10 minutes on ice and neutralized with 150 μL of 1 mol/L Tris–HCl (pH 9.0). After centrifugation, the supernatant was collected, and the cells in the precipitate were washed once with PBS-BSA and lysed with 0.1% Triton X-100 for 2 hours at room temperature. Thus, the internalized phages in the cell lysate were recovered. A total of 10 μL of eluted phage was titrated on agar plates in the presence of IPTG/X-gel (1 mg/L) and tetracycline (40 mg/mL). The remaining phages were amplified by ER2738 bacteria at 37°C for 4.5 hours and injected into tumor-bearing mice. The biopanning process was repeated for three rounds. At the end of the third round, the phage solution was eluted and titrated on LB/IPTG/X-gel plates. Then, 20 single blue colonies were randomly picked from the phage titer plates, followed by amplification and stored at −4°C (17). For ELISA, RT112 and SV-HUC-1 cells were plated at 1×10^4 cells/well in a 96-well plate and incubated at 37°C in 5% CO_2 for 24 hours. Subsequently, cells were washed and fixed with 4% paraformaldehyde for 15 minutes at room temperature. After incubation with 3% H_2O_2 (100 μL/well) at 37°C for 30 minutes, the plates were washed 3 times with PBS, and the wells were blocked with 200 mL of 5% BSA for 30 minutes at 37°C. The phages (1×10^{10} PFU/well) were added to RT112 or SV-HUC-1 cells and incubated at 37°C for 2 hours. The plates were then washed 3 times with TBST before the addition of 100 μL of HRP-anti-M13 mAb (1:5,000) for 1 hour at 37°C. After washing 3 times with 0.05% TBST, 3,3′,5,5′-tetramethylbenzidine (TMB) was added at room temperature for 30 minutes. The reaction was terminated by the addition of 50 μL of 2 mol/L H_2SO_4. Subsequently, absorbance was read using an automated ELISA plate reader at 450 nm. Unrelated phages with equal titers were added to the wells in place of selected phage clones to serve as negative controls. Selectivity was determined using the following formula: $\text{Selectivity} = [\text{RT112}(OD_{450} - OD_{450\text{negative control}})]/[\text{SV-HUC-1}(OD_{450} - OD_{450\text{negative control}})]$.

DNA sequencing and peptide synthesis

The selected clone was sequenced using a DNA sequencer according to previously described protocols (18). CSDRIMRGC (PLSWT7) and control CQRSPIHDC (cPLSWT7) peptides were synthesized (Chinese Peptide Co.) using standard solid-phase fluorenylmethyloxycarbonyl chloride chemistry. The products were purified by high-performance liquid chromatography and stored at −20°C. Synthesis and characterization of the

Published OnlineFirst August 6, 2018; DOI: 10.1158/1535-7163.MCT-18-0212

IRDye800CW-labeled peptide (PLSWT7-DMI) are described in the Supplementary Information.

PLSWT7-DMI metabolic profile and competition assay *in vivo*

PLSW7-DMI or cPLSWT7-DMI (500 μL, 180 pmol/mL) was instilled into the pouches of APBC mice. After 30 minutes, extra probes were washed out twice with PBS, and *in vivo* fluorescence images were acquired using the IVIS Spectrum imaging system (Xenogen) at 0.5, 1, 2, 3, 4, and 6 hours. Tumors and organs were then harvested for *ex vivo* imaging. For all imaging acquisitions, mice were anesthetized using a 3% isoflurane/air mixture The homing ability of the probe to the tumor following intravenous administration was also assessed. PLSW7-DMI or cPLSWT7-DMI (150 μL, 1.8×10^4 pmol/mL) was injected intravenously into mice in the two groups. Then, *in vivo* fluorescence images were acquired at 0, 1, 3, 8, 12, 24, and 36 hours using the IVIS Spectrum imaging system.

For *in vivo* competition assays, free PLSWT7 peptides were instilled into the pouches of APBC mice or the bladders of orthotopic bladder cancer mice prior to PLSWT7-DMI instillation. Images were obtained using a homemade near-infrared (NIR)-imaging system, and mean fluorescence density was quantified using Image Pro Plus 6.0 (Media Cybernetics, Inc.).

Fibered confocal fluorescence microscopy (FCFM) studies

The intratumor distribution of PLSWT7 was evaluated by FCFM imaging (Cellvizio; Mauna Kea Technologies). PLSWT7-fluorescein isothiocyanate (FITC) was instilled into the pouches of APBC mice. After 30 minutes, the pouches were washed twice with PBS, and a small incision (~0.5 cm) was made to insert the laser fiber. Evans blue was injected through the tail vein before FCFM imaging to visualize blood vessels. All imaging was performed at a frame rate of 9 Hz (full field of view), a field of view of 618 × 609 μm, and 100% laser power at 488 nm and 660 nm. Images and videos were analyzed using a Cellvizio Dual Viewer (Mauna Kea Technologies).

PAI *in vivo*

In vivo mouse imaging studies were performed using a real-time multispectral optoacoustic tomography (MSOT) imaging system (inVision 128; iThera Medical GmbH). An optical parametric oscillator operating from 740 nm to 800 nm (excitation wavelengths: 740, 750, 760, 780, 790, and 800 nm) was pumped using a Q-switched Nd:YAG laser with a 10-ns pulse duration and a 10-Hz repetition rate. Light was directed into a fiber bundle containing 10 individual fibers, and PA signals were obtained using a 128-element concave transducer array spanning a circular arc of 270°.

Probes were instilled into APBC or orthotopic bladder cancer mice. After 30 minutes, extra probes were washed out twice with PBS, and ultrasound gel was applied onto the mouse skin. Multiple cross-sections of mice were performed in a water tank with the imaging chamber on a horizontal plane. The ultrasonic coupling gel was applied to mice under deep anesthesia, and the mice were loaded into a plastic membrane for protection from water. APBC or orthotopic bladder cancer mice in the supine position were scanned with a step size of 0.2 mm spanning from the abdomen to the lower limbs. Subcutaneous tumor-bearing mice were also subjected to PAI 8 hours after probe injection via the tail vein, following the procedure described above. Images were reconstructed by multispectral processing using MSOT (iThera Medical GmbH), and the entire tumor site was used to analyze PAI-signal intensity. For the selected region, the PAI signal was summed and averaged. After photoacoustic imaging, the air pouches of tumor-bearing mice were opened, tumor lesions were located, and the size was measured.

NIR fluorescence-imaging-guided surgery and residual verification

Thirty minutes before tumor resection, APBC mice were instilled with PLSWT7-DMI into their pouches, and extra probes were washed out with PBS. Following anesthetization, a genito-urinary surgeon removed the tumors using a homemade intraoperative NIR-imaging system for guidance. Residual tumors were visualized in real-time and were gradually resected. Harvested tissues were subjected to histologic examination.

Recurrence and survival-rate analyses

Following PLSWT7-DMI instillation and anesthetization, surgery was performed on APBC mice with tumors ≥5 mm using a partial resection procedure (19). The mice were divided into surgery only ($n = 20$) and surgery plus imaging ($n = 20$) groups and used for recurrence and survival-rate analyses.

Ex vivo imaging of human bladders

After obtaining Institutional Review Board approval from The Fourth Hospital of Harbin Medical University (YXLLSC-2017-09), patients with urothelial carcinoma ($n = 8$) scheduled for radical cystectomy were selected and informed consent was obtained. After radical cystectomy, bladder specimens were immediately removed, cut open, and washed three times with 0.9% saline solution. The bladder was first sprayed with the control (cPLSWT7-DMI), and after 30 minutes, images were obtained using the homemade endoscopy system. After washing, the bladder was resprayed with PLSWT7-DMI and images were obtained. Mean fluorescence density was quantified using Image Pro Plus 6.0 (Media Cybernetics, Inc.).

Statistical analysis

Data were analyzed using SPSS (v.20; IBM Corp.). Results are presented as means ± standard deviations (SD) for experiments performed in triplicate. Two-tailed, independent, two-sample *t* tests were used to assess differences in fluorescence intensities and tumor-to-background ratios between groups. Differences were considered statistically significant at $P < 0.05$.

Details of the *in vitro* experiments are presented in the Supplementary Information.

Results

Phage-display selection of the bladder cancer cell–specific peptide

To select peptides with high specificity for bladder cancer cells, phage recovery from xenograft tumor tissues was assessed after each round of biopanning. The number of phages specifically bound to the tumor gradually increased and was enriched 3.66×10^3-fold after the third round of screening as compared with the first round (Supplementary Table S1).

In the last round of selection, 20 individual phage clones were identified and evaluated by ELISA to identify clones exhibiting high RT112 selectivity. Phage clone P7 exhibited the highest RT112 selectivity (13.24), indicating preferential binding to the human bladder cancer cell line (Fig. 1A). Therefore, P7 was

Published OnlineFirst August 6, 2018; DOI: 10.1158/1535-7163.MCT-18-0212

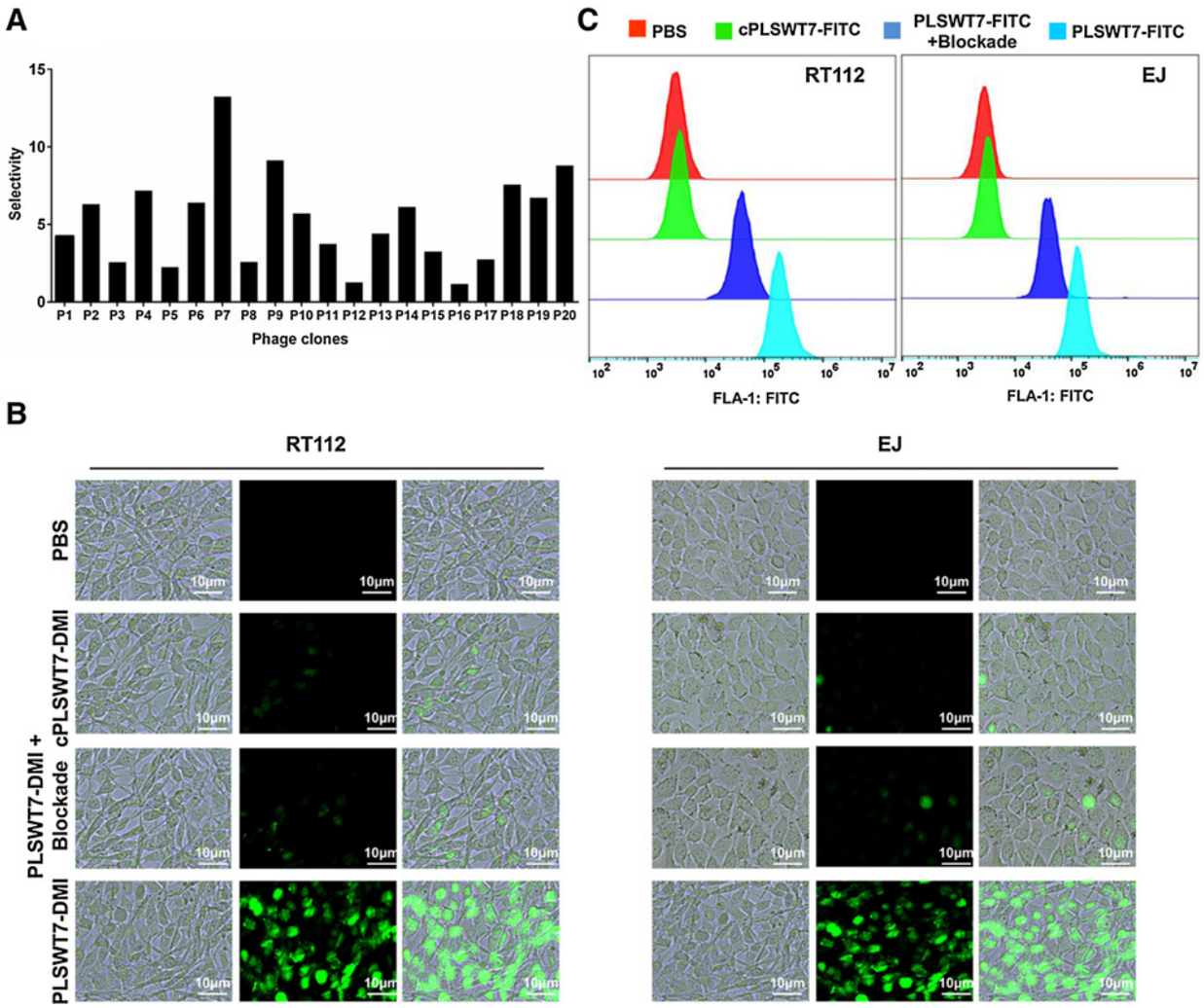

Figure 1.

Phage-display selection of bladder cancer–cell-targeted peptides. **A,** The selectivity of phage clones to RT112 cells determined by ELISA. Phage clone P7 showed the highest selectivity. **B,** Fluorescence microscopy images of RT112 and EJ cells incubated with PBS, cPLSWT7-DMI, PLSWT7-DMI with blockade, or PLSWT7-DMI. The PLSWT7-DMI–treated group showed higher binding affinity than those of other groups. **C,** Flow-cytometric analysis of RT112 and EJ cells incubated with PBS, cPLSWT7-FITC, PLSWT7-FITC with blockade (PLSWT7), or PLSWT7-FITC. The PLSWT7-FITC–treated group exhibited higher fluorescence intensity than those of other groups.

isolated, sequenced, and translated into a corresponding peptide (PLSWT7), followed by labeling with IRDye800CW (PLSWT7-DMI) or FITC. The fluorescence spectra, stability, and biocompatibility of PLSWT7-DMI are shown in Supplementary Fig. S1. Cells incubated with 180 pmol/mL PLSWT7-DMI produced the highest fluorescence intensity (Supplementary Fig. S1D). To evaluate specificity, RT112, EJ, and SV-HUC-1 (a normal urothelium cell line), cells were incubated with the probes and high fluorescence signals were observed in tumor cells incubated with PLSWT7-DMI, indicating efficient binding to RT112 and EJ cells. However, no fluorescence was observed following incubation with cPLSWT7-DMI or PBS. Additionally, pretreatment with PLSWT7 prevented PLSWT7-DMI from binding (Fig. 1B) and minimal fluorescence signals were observed in SV-HUC-1 cells incubated with PLSWT7-DMI (Supplementary Fig. S2), suggesting that the binding of PLSWT7-DMI occurred through targeting to specific sites on tumor cells. To quantitatively evaluate probe bind with bladder cancer cells, we performed quantitative flow cytometry on bladder cancer cells. On average, tumor cells incubated with PLSWT7-FITC exhibited a prominent right shift upon cytometric analysis, suggesting a much higher affinity of the probes than that of their blocked and nontargeting counterparts (Fig. 1C).

PLSWT7-DMI metabolic profile

To evaluate the PLSWT7-DMI metabolic profile after instillation, we instilled probes into the pouches of the APBC mouse model, rinsed extra probes after 30 minutes, and obtained images at various time points. For mice instilled with PLSWT7-DMI, probe-specific accumulation was observed at 0.5 hours after

Published OnlineFirst August 6, 2018; DOI: 10.1158/1535-7163.MCT-18-0212

instillation (Fig. 2A) and the signal in tumors peaked followed by a gradual decline. The retention time was up to 6 hours (Fig. 2B). Compared with mice instilled with nontargeting cPLSWT7-DMI, the PLSWT7-DMI–treated group exhibited a higher signal at every time point and a longer retention time, indicating high specificity *in vivo*. In addition, subcutaneous tumor-bearing mice that received PLSWT7-DMI or cPLSWT7-DMI via tail-vein injection were evaluated by IVIS at various time points. The PLSWT7-DMI group displayed better optical contrast and longer retention times than those of the cPLSWT7-DMI group in the tumor region (Supplementary Fig. S3A). The PLSWT7-DMI group showed a stronger optical signal in the tumor region at all time points than those of the cPLSWT7-DMI group (Supplementary Fig. S3B). Significantly different tumor-to-background ratio (TBR) profiles

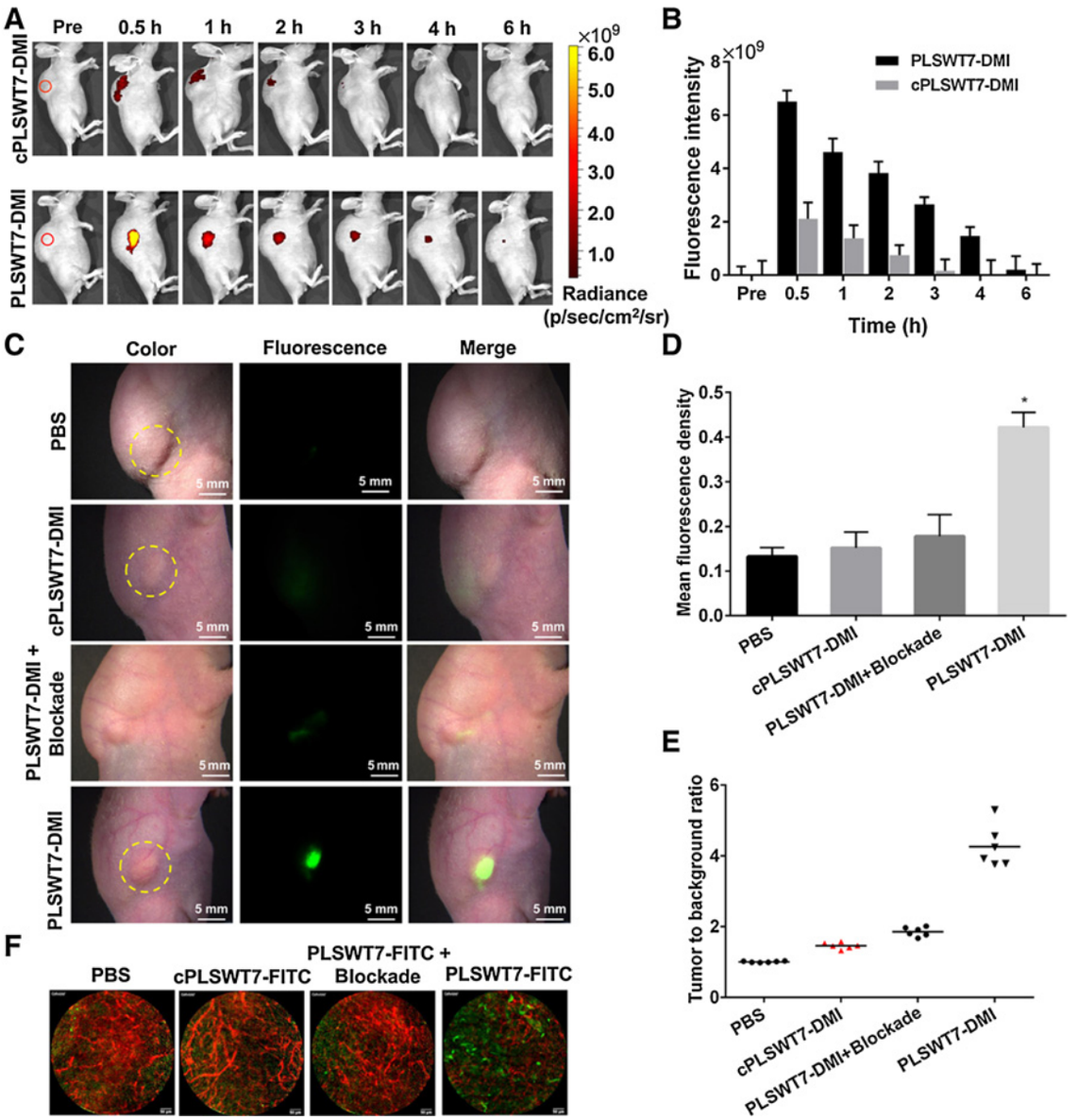

Figure 2.

Metabolic profile of PLSWT7-DMI. **A,** IVIS imaging of APBC mice instilled with cPLSWT7-DMI or PLSWT7-DMI at different time points. Red circle indicates tumor region. **B,** Fluorescence intensity of the tumor site in **A**. Fluorescence intensity peaked after instillation and gradually decreased. The PLSWT7-DMI–treated group exhibited a higher fluorescence intensity and longer retention time than those of controls. **C,** NIR imaging of APBC mice. Pouches of APBC mice were instilled with PBS, cPLSWT7-DMI, PLSWT7-DMI with blockade, or PLSWT7-DMI, followed by imaging using a homemade NIR-imaging system at 30 minutes after instillation. Tumors in the PLSWT7-DMI–treated group were clearly visualized; however, blockade of PLSWT7-DMI binding was observed after PLSWT7 pretreatment. The yellow-dashed circle indicates the tumor site. The PLSWT7-DMI groups displayed a markedly higher (**D**) mean fluorescence density and (**E**) TBR. **F,** FCFM imaging showed that probe accumulation was unrelated to blood-vessel intensity. Green fluorescence indicates probes; red fluorescence indicates blood vessels. Values are presented as means ± SD of 5 animals. *, $P < 0.05$ vs. PLSWT7-DMI + blockade groups.

Published OnlineFirst August 6, 2018; DOI: 10.1158/1535-7163.MCT-18-0212

were observed between the groups (Supplementary Fig. S3C). Notably, the TBR peak of the PLSWT7-DMI group (8.84 ± 0.6) appeared at 8 hours after injection and was ∼1.35-fold higher than that of the cPLSWT7-DMI group (6.57 ± 0.5). Accordingly, PLSWT7-DMI administered by instillation or intravenous injection both exhibits higher *in vivo* targeting ability for bladder cancer.

To further confirm the bladder cancer tumor specificity of PLSWT7-DMI, we performed a competition assay using our homemade NIR-imaging system. PLSWT7 peptides were instilled into the pouches of APBC mice or the bladders of orthotopic bladder cancer mice prior to probe instillation. There was little accumulation of PLSWT7-DMI after instillation, indicating effective competition and selectivity of the probe bound to the tumors *in vivo* (Fig. 2C). Additionally, the PLSWT7-DMI–treated group exhibited significantly higher fluorescence intensity and TBR in both APBC (Fig. 2D and E) and orthotopic models (Supplementary Fig. S5B and S5C) than those of other groups. A negligible signal was observed in nontumor areas (Fig. 2A), suggesting that few probes entered the bloodstream and began circulating in the body after instillation. Based on FCFM imaging of tumors in the APBC model, the level of probe accumulation was unrelated to tumor blood-vessel density (Fig. 2F), presumably because the probes were administered by instillation, rather than by systematic administration, and accumulated on the surface of the tumor, with minimal entry into circulation. After 6 hours, mice were sacrificed, organs were harvested, and fluorescence intensity was measured. A bright signal was observed in RT112 tumors, whereas signals in organs were minimal (Supplementary Fig. S4A and S4B).

PLSWT7-DMI–based PAI for bladder cancer diagnosis

Because PLSWT7-DMI bound specifically to bladder cancer tumors *in vivo*, we verified the utility of the probe for bladder cancer PAI diagnosis in APBC and orthotopic models. Tumor-bearing pouches or bladders were instilled with probes, followed by PAI. Signals were significantly higher in the PLSWT7-DMI–treated groups than in other groups, and tumors <3 mm in the PLSWT7-DMI–treated group could be clearly visualized (Fig. 3A), consistent with the results for the orthotopic model (Fig. 3B). Additionally, the signal intensity was significantly higher in the PLSWT7-DMI–treated group than in other groups (Fig. 3C and D). These results indicated that PLSWT7-DMI–based PAI could be applied for the diagnosis of small foci. We also verified the utility of the probe for bladder cancer PAI in tumor-bearing mice that received PLSWT7-DMI or cPLSWT7-DMI via tail-vein injection. Enhanced contrast was observed in PLSWT7-DMI–treated groups compared with other groups (Supplementary Fig. S6A). Furthermore, the signal intensity was significantly higher in the PLSWT7-DMI–treated group than in other groups (Supplementary Fig. S6B). These results suggested that PLSWT7-DMI–based PAI could be applied for bladder cancer diagnosis after instillation or intravenous injection.

NIR-imaging–guided surgery and residual tumor detection

Thirty minutes after PLSWT7-DMI instillation, the tumor was illuminated at high optical contrast, followed by the gradual removal of the illuminated lesions (Fig. 4A). Suspected residuals were effectively detected and resected, including those that were difficult to discriminate under white light, such as inflammatory lesions (Fig. 4A, site b) and small foci <0.5 mm in diameter (Fig. 4A, site c). To validate the accuracy of tumor-margin definition using PLSWT7-DMI, the surgeon deliberately resected a piece of tissue containing both fluorescent and nonfluorescent regions. Hematoxylin and eosin (H&E) staining confirmed the ability of PLSWT7-DMI to delineate tumor margins (Fig. 4B, section a), discriminate between tumors and inflammatory lesions (Fig. 4B, section b), and recognize small foci (Fig. 4B, section c). An overlay of the NIR-fluorescent image and H&E staining demonstrated consistent tumor-margin definition at the microscopic level (Fig. 4B, section a).

We harvested organs and pouches to evaluate the biocompatibility of PLSWT7-DMI *in vivo*. H&E staining showed no damage to major organ structures (Fig. 4C) and no difference in the number of inflammatory cells penetrating the air pouches (Fig. 4D). Additionally, the mRNA expression levels of proinflammatory factors, e.g., interleukin (IL)-1β and tumor necrosis factor (TNF)-α, did not differ between groups (Fig. 4E). These results indicated that PLSWT7-DMI did not cause cytotoxicity or cystitis and is potentially safe for clinical application.

NIR-imaging–guided tumor resection prevents bladder cancer recurrence

Following anesthetization and PLSWT7-DMI instillation, surgery was performed on APBC mice with tumors ≥5 mm ($n = 45$) using a partial resection procedure (19). Briefly, an approximately 2-cm incision was made adjacent to the tumor, and 95% of the tumor was removed. Two additional surgeons visually examined all mice and excluded five that had obvious residual tumors or positive margins. This procedure was performed to mimic small residuals that could not typically be visually detected. The remaining mice were divided into surgery only ($n = 20$) and surgery plus imaging ($n = 20$) groups. This procedure guarantees that mice in the surgery plus imaging group have undetectable small residuals and thereby avoids unintentional bias that would lead to poorer resection in the nonimaging group. Mice in the surgery group had their wounds closed and were observed. In the surgery plus imaging group, PLSWT7-DMI–based NIR-imaging-guided tumor resection was conducted (Fig. 5A). After 1 week, IVIS imaging revealed that 19 of 20 mice in the surgery group showed tumor recurrence, whereas only 1 mouse in the surgery plus imaging group showed tumor recurrence (Fig. 5B and C). Over the 30-day postoperative follow-up, mice that underwent probe-guided tumor resection showed a significant survival advantage over mice that underwent surgery only (Fig. 5D). Two mice in the surgery plus imaging group died during follow-up, one due to tumor recurrence and the other due to a wound infection.

Ex vivo NIR imaging of the human bladder

To evaluate the translational potential of PLSWT7-DMI, we monitored the binding of PLSWT7-DMI to tumors in fresh human bladders using our homemade endoscopic system. Patient characteristics and final pathologic diagnoses are provided in Supplementary Table S2. After radical cystectomy, bladder specimens were immediately removed, cut open, and washed three times with 0.9% saline solution. The bladder was then sprayed with control (cPLSWT7-DMI) and imaged by a homemade NIR endoscopy. After washing, the bladder was resprayed with PLSWT7-DMI and imaged again. Under white light, tumor sites were difficult to recognize (Fig. 6A), and it was challenging to delineate the extent of the tumor (Fig. 6A, case #1), recognize easily overlooked foci (Fig. 6A, case #2), discriminate between malignant and benign

Published OnlineFirst August 6, 2018; DOI: 10.1158/1535-7163.MCT-18-0212

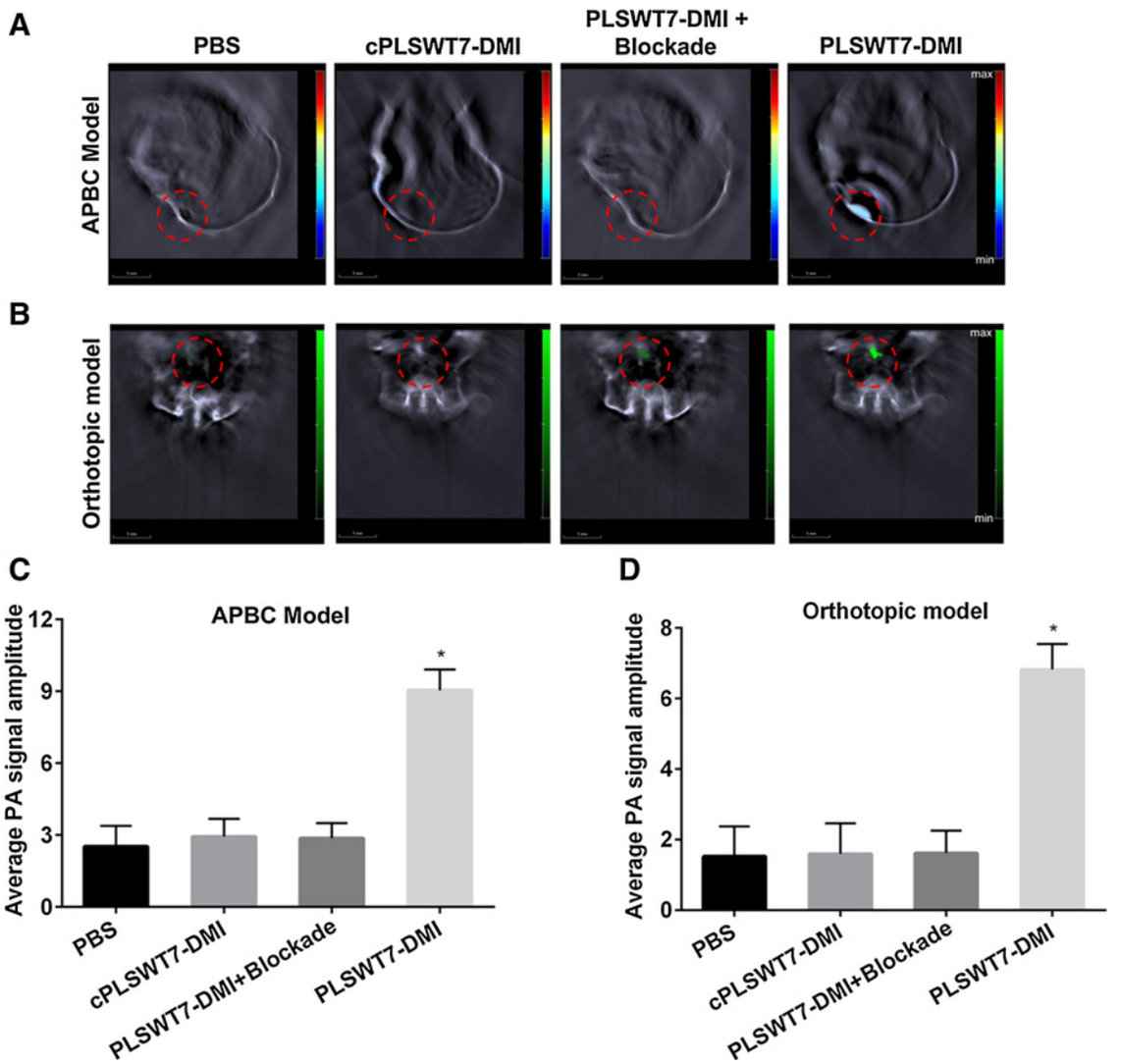

Figure 3.

PAI of APBC and orthotopic bladder cancer mice. **A,** PAI of APBC mice. Pouches of APBC mice were instilled with PBS, cPLSWT7-DMI, PLSWT7-DMI with blockade, or PLSWT7-DMI, followed by PAI. The PLSWT7-DMI–treated group exhibited a better contrast than other groups. The red-dashed circle indicates the tumor site. **B,** PAI of orthotopic bladder cancer mice. Bladders of orthotopic bladder cancer mice were instilled with PBS, cPLSWT7-DMI, PLSWT7-DMI with blockade, or PLSWT7-DMI, followed by PAI. The PLSWT7-DMI–treated group exhibited a better contrast than other groups. The red-dashed circle indicates the tumor site. Quantification of the average PA-signal amplitude of (**C**) APBC mice or (**D**) orthotopic bladder cancer mice in **A** and **B**. The PLSWT7-DMI–treated group exhibited higher signals than other groups. Values are presented as means ± SD of 5 animals. *, $P < 0.05$ vs. PLSWT7-DMI + blockade groups.

lesions (Fig. 6A, case #3), and detect flat neoplasms (Fig. 6A, case #4). For the control, no contrast was detected between normal and tumor-appearing mucosae (Supplementary Fig. S7). After incubation with PLSWT7-DMI, tumors were clearly illuminated, but the normal mucosa was not, indicating specific targeting of the probe. Quantitative analysis showed that the fluorescence density was significantly higher in the tumor than in the normal mucosa after incubation with PLSWT7-DMI, with no difference post-cPLSWT7-DMI administration (Fig. 6C). Under probe-based NIR imaging, the extent of the tumor was clearly delineated, and easily overlooked foci such as small foci and carcinoma *in situ* were visualized (Fig. 6A, cases #1, 2, and 4). Additionally, benign lesions were easily discriminated because the probe bound only to tumor tissues (Fig. 6A, case #3). Histopathology subsequently confirmed these findings (Fig. 6B).

Overall, 40 bladder regions were analyzed for a comparison of PLSWT7-DMI–based NIR-imaging diagnosis with histopathology (Supplementary Table S3). True-positive probe binding was found in 21 of 25 biopsies with histologically confirmed cancer (sensitivity, 84%), whereas 13 of 15 benign biopsies were true negatives, with no evidence of probe binding (specificity, 86.7%). For NMIBC, 18 of 20 biopsies were true positive with PLSWT7-DMI binding. For MIBC, 3 of 5 biopsies were true positives. These results suggested that PLSWT7-DMI could specifically bind to human bladder cancer tissues and thus hold great potential for clinical translation.

Published OnlineFirst August 6, 2018; DOI: 10.1158/1535-7163.MCT-18-0212

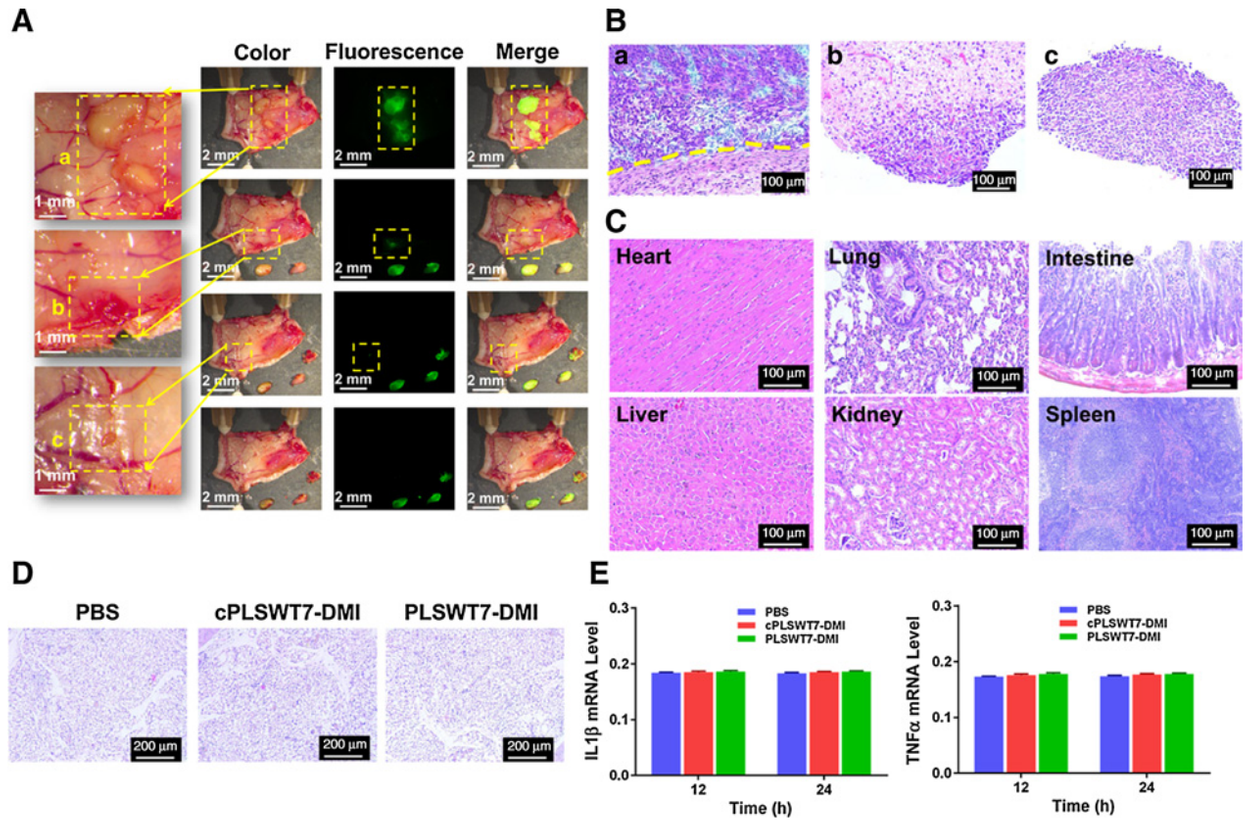

Figure 4.

NIR-imaging–guided surgery in APBC mice and histologic analysis. **A,** Tumors were gradually removed using NIR-imaging–guided surgery. Tumor margins were clearly delineated (site a), tumors and inflammatory lesions (site b) were easily discriminated, and small foci <0.5 mm (site c) were recognized. **B,** H&E staining of corresponding tissues resected in **A**. For sections from site a, white-light and fluorescence microscopy images were both acquired, with an overlay of the images demonstrating consistent tumor-margin definition at the microscopic level. The yellow-dashed line indicates the tumor margin. Sections from sites b and c were confirmed as a malignant lesion and residual tumor, respectively. **C,** H&E staining of organs. No damage was observed to organ structures after PLSWT7-DMI instillation. **D,** H&E staining of air pouches. No difference in the number of inflammatory cells penetrating air pouches after PLSWT7-DMI instillation was observed relative to controls. **E,** mRNA expression of *IL1β* and *TNFα* in air pouches. No differences in the mRNA expression levels of the proinflammatory factors *IL1β* and *TNFα* were observed among PBS-, cPLSWT7-DMI–, and PLSWT7-DMI–treated groups. Values are presented as means ± SD of 5 animals.

Discussion

The purpose of this study is to developed a bladder cancer–specific probe (PLSWT7-DMI) and applied it for PAI diagnosis and NIR-imaging–guided surgery after instillation. Probes were instilled into an APBC mouse model and human bladders to mimic intravesical administration used in clinical practice. The tumor-specific peptide PLSWT7 was selected by phage-display technology. Several peptides, such as CSNRDARRC (20), PLZ4 (21), and NYZL1 (16), show effective binding activity with bladder cancer–specific tumors; however, CSNRDARRC and PLZ4 were screened from muscle-invasive bladder cancer cell lines, whereas NMIBC accounts for 70% of all patients with bladder cancer. NYZL1 was screened from NMIBC cell lines, but *in vivo* studies are lacking.

The tumor-targeting peptide selected from the Ph.D.-C7C phage-display peptide library is a cyclic peptide that shows better biological activity than that of their linear counterparts due to conformational rigidity (22). Additionally, the cyclic structure is resistant to hydrolysis by exopeptidases due to the lack of both amino and carboxy termini. We identified a phage-display derived peptide-based probe (PLSWT7-DMI) that can specifically bind and be taken up by bladder cancer cells (RT112 and EJ). The effective binding of PLSWT7-DMI to bladder cancer cells indicated its potential for targeted therapeutic and imaging approaches.

To evaluate the translational potential of PLSWT7-DMI, the probe should be administered via the same route used to deliver pharmacologic agents in clinical practice. As an easily accessible hollow organ, the bladder provides a well-established route for the instillation of pharmacologic agents (intravesical administration; ref. 23). The bladder cancer mouse models described to date were unsuitable for instillation because subcutaneous models provide no space for perfusion, and the establishment of orthotopic models is associated with high death rates (24). Therefore, we established an air-pouch on the back of mice and implanted the tumor on the pouch to mimic tumor growth on the bladder wall. We then instilled the probes into the pouch and found that PLSWT7-DMI specifically accumulated on the bladder cancer tumor and exhibited significantly higher signal intensities than those of controls. A competition study further demonstrated probe specificity, with fluorescence intensity decreasing by

Published OnlineFirst August 6, 2018; DOI: 10.1158/1535-7163.MCT-18-0212

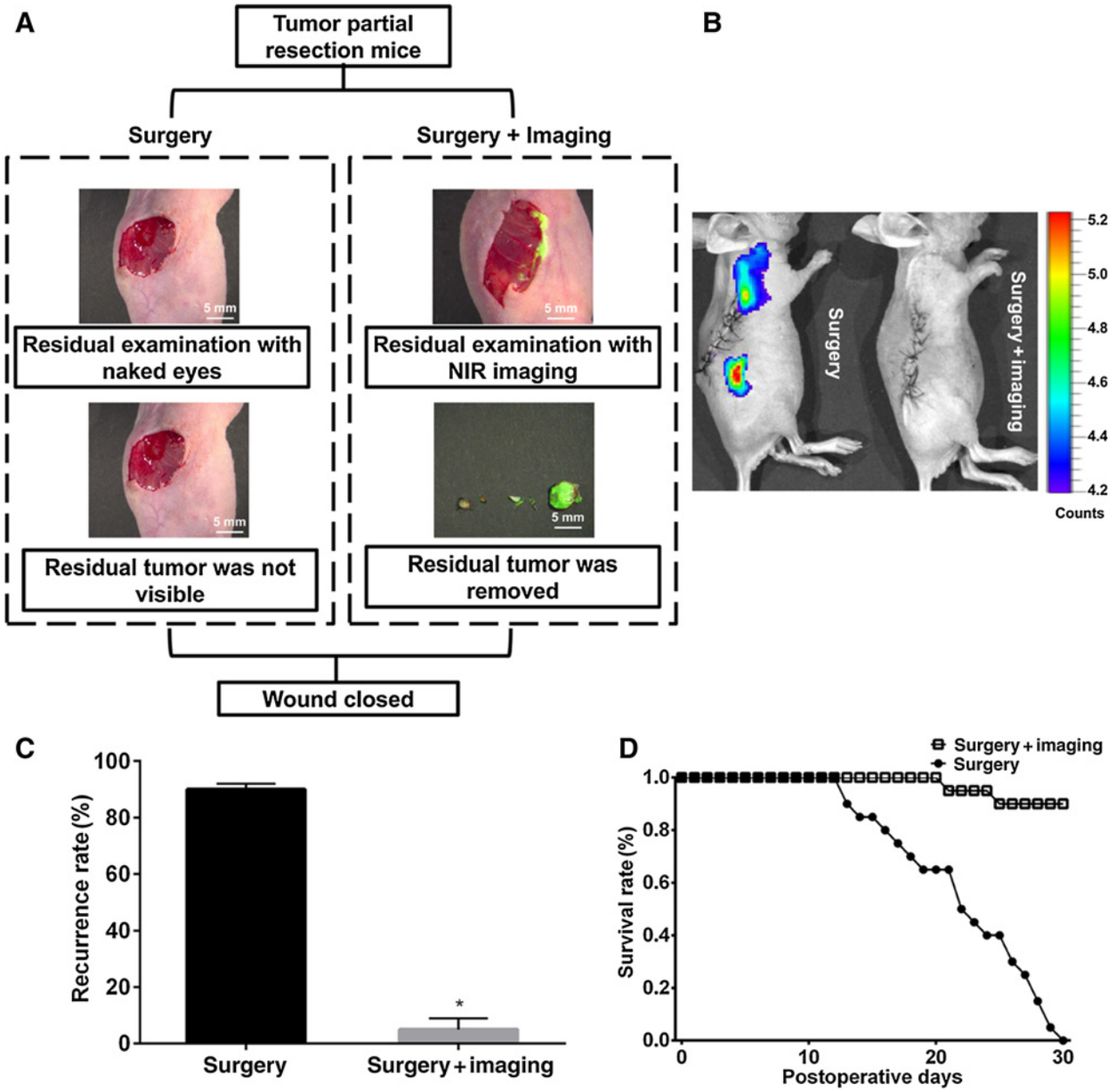

Figure 5.

NIR-imaging–guided tumor resection prevents bladder cancer recurrence. **A,** Residual tumor detection in APBC mice. In the surgery group ($n = 20$), residuals could not be detected by the naked eye. Mice had their wounds closed. In the surgery plus imaging group ($n = 20$), tumor residuals were visualized under NIR imaging and probe-based NIR-imaging–guided tumor resection was conducted. **B,** IVIS imaging of tumor recurrence in the surgery and surgery plus imaging groups 1 week after surgery. Tumor relapse was observed in the surgery group, but not in the surgery plus imaging group. **C,** A 90% lower recurrence rate was observed in the surgery plus imaging group than in the surgery group. **D,** Plot of the survival rate postoperation for the surgery and surgery plus imaging groups. Over the 30-day postoperative follow-up, mice that underwent imaging-guided tumor resection showed a significant survival advantage over mice that underwent surgery only. Values are presented as means ± SD of 20 animals. *, $P < 0.05$ vs. surgery groups.

57.8% when mice were pretreated with a blocking peptide (PLSWT7). We also evaluated probe metabolic profiles after intravenous injection and found that it required hours to reach the highest TBR, whereas fluorescence intensity and TBR reached peaks at 30-minutes after instillation using our approach. This might be explained by the immediate binding of the probe to a specific site on the tumor upon probe-solution attachment to the tumor surface, unlike delivery by circulation following systemic administration. Although instillation of PLSWT7-DMI resulted in relatively faster clearance than systemically administered probes, 6 hours was sufficient for surgeons to perform the operation. Additionally, we observed negligible signal intensity in other organs, indicating minimal systemic absorption and few potential side effects.

Published OnlineFirst August 6, 2018; DOI: 10.1158/1535-7163.MCT-18-0212

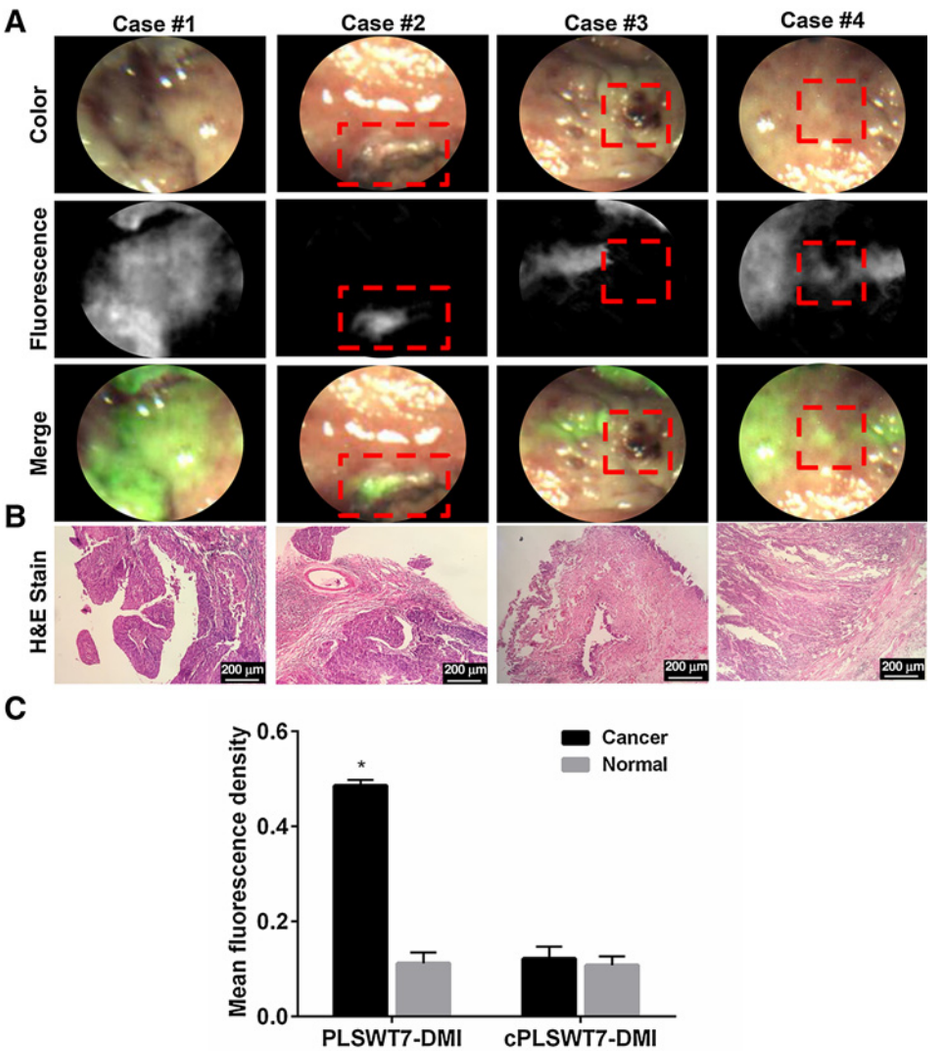

Figure 6.
Ex vivo PLSWT7-DMI–based NIR imaging of human bladders. **A,** PLSWT7-DMI–based NIR endoscopy imaging allowed the delineation of the tumor extent (case #1), visualization of small foci (case #2) and flat neoplasms (case #4), and easy differentiation of benign lesions (case #3). Red-dashed squares indicate small foci in case #2, benign lesion in case #3, and flat neoplasm in case #4. **B,** Histopathology confirmed the above findings. **C,** Mean fluorescence density in cancer and normal tissues postadministration of PLSWT7-DMI or cPLSWT7-DMI. Values, means ± SD of 8 cases. *, $P < 0.05$ vs. normal tissues.

Current bladder cancer diagnosis and treatment methods are inadequate to detect small foci and to identify the extent of malignancy, contributing to the high recurrence rate. Conventional ultrasound is a low-cost and noninvasive technique (25), but has a low resolution and specificity (26), making it insufficient for bladder cancer diagnosis, especially for small tumors. PAI provides better spatial resolution than conventional ultrasound (27). When combined with targeted probes, e.g., gold nanoparticles and carbon nanotubes (28), PAI can be applied for tumor-specific diagnosis. The PLSWT7-DMI–based PAI detected tumors <3 mm in diameter with desired contrast and resolution. However, because the PA signal cannot travel through air, the APBC model is not convincing for PAI evaluation; therefore, we evaluated PAI in an orthotopic bladder cancer model. Although the signal amplitude was lower than that in the APBC model, small tumors could be easily recognized, suggesting that surgeons would be able to detect and remove the tumor before the condition worsened. Moreover, the high level of tissue penetration makes PAI a promising approach for preoperative bladder cancer diagnosis; however, precise intraoperative tumor delineation via PAI is difficult and an optical signal might be beneficial. Therefore, the NIR-imaging modality of PLSWT7-DMI was applied for tumor resection.

Conventional WLC- and HAL-based blue-light fluorescence cystoscopy are valuable imaging tools for minimally invasive transurethral resection in NMIBC. However, randomized clinical trials and meta-analyses suggest that these approaches have limited sensitivity and specificity in guiding surgeons to achieve precise bladder cancer resection (29). Here, successful intraoperative imaging-guided bladder cancer resection in mouse model demonstrated that PLSWT7-DMI could help surgeons (i) define the exact extent of the tumor; (ii) discriminate between malignant and benign lesions; and (iii) check for residual tumors, even those <0.5 mm, during the operation (Fig. 4). These issues contribute to tumor recurrence after conventional tumor resection (30, 31) because surgeons can solely depend upon their eyes to visualize tumor tissue. We demonstrated a significant reduction in the recurrence rate and an increase in survival in mice simply by examining the surgical wound for residual disease and using probe-based NIR-imaging–guided resection prior to wound closure. To assess the potential of PLSWT7-DMI for clinical translation, we conducted probe-based NIR-imaging in *ex vivo* human

Published OnlineFirst August 6, 2018; DOI: 10.1158/1535-7163.MCT-18-0212

bladders. The specificity and sensitivity of probe-based NIR-imaging were 86.7% and 84%, which are much higher than those for WLC (specificity = 25%, sensitivity = 66.67%; ref. 32). Easy-to-overlook lesions, such as small foci and flat neoplasms, are the leading cause of bladder cancer recurrence. Using PLSWT7-DMI, these lesions were clearly visualized. Interestingly, although PLSWT7-DMI was selected from an NMIBC cell line, it was also capable of binding to MIBC tissues (Fig. 6), suggesting the PLSWT7-DMI–binding site is present in both NMIBC and MIBC tissues. This hypothesis requires further exploration. Furthermore, we did not perform transurethral endoscopic examination due to the large diameter of our homemade endoscope.

In conclusion, we developed a phage-display–derived, highly specific probe for bladder cancer PAI diagnosis and NIR-imaging–guided resection. PAI enables the preoperative detection of small tumor foci with fine spatial resolution, and NIR imaging allows the visualization of the tumor extent and residuals, thereby assisting in intraoperative bladder cancer resection. This approach holds great potential for clinical translation but some limitations need to be addressed: (i) the lack of NIR cystoscopy for NIR-imaging–guided bladder cancer resection; (ii) the unknown depth of tumor infiltration because the probe only accumulates on the surface of the tumor postinstillation; and (iii) the unknown side effects of PLSWT7-DMI in humans, particularly with respect to the immunogenic response. Future investigations will include evaluations of the use of this probe in routine clinical practice and its impact on bladder cancer recurrence.

Disclosure of Potential Conflicts of Interest

No potential conflicts of interest were disclosed.

Authors' Contributions

Conception and design: L. Peng, W. Shang, W. Xu
Development of methodology: L. Peng, W. Shang, P. Guo, K. Wang
Acquisition of data (provided animals, acquired and managed patients, provided facilities, etc.): L. Peng, W. Shang, H. Wang
Analysis and interpretation of data (e.g., statistical analysis, biostatistics, computational analysis): L. Peng, W. Shang, Z. Han, H. Jiang
Writing, review, and/or revision of the manuscript: L. Peng, J. Tian, W. Xu
Administrative, technical, or material support (i.e., reporting or organizing data, constructing databases): P. Guo, K. He, J. Tian, K. Wang
Study supervision: J. Tian, W. Xu

Acknowledgments

This work was supported by the National Natural Science Foundation of China under Grant Nos. 81270022 (to W.H. Xu), 81227901 (J. Tian), 61231004 (J. Tian), 81501540 (W.T. Shang), 61671449 (K. Wang); the National Key R&D Program of China No. 2017YFA0205200 (J. Tian); the Strategic Priority Research Program from Chinese Academy of Sciences under Grant No. XDB02060010 (J. Tian); the Beijing Municipal Science & Technology Commission under Grant No. Z161100002616022 (J. Tian); Natural Science Foundation of Heilongjiang Province of China: QC2017097 (L. Peng). We would like to thank Tongtong (Key Laboratory of Molecular Imaging, Institute of Automation, Chinese Academy of Sciences) for his supervision and advice regarding the PAI and Kun Su (Key Laboratory of Molecular Imaging, Institute of Automation, Chinese Academy of Sciences) for technical support regarding the application of equipment.

The costs of publication of this article were defrayed in part by the payment of page charges. This article must therefore be hereby marked *advertisement* in accordance with 18 U.S.C. Section 1734 solely to indicate this fact.

Received February 23, 2018; revised May 9, 2018; accepted August 2, 2018; published first August 6, 2018.

References

1. Chen W, Zheng R, Baade PD, Zhang S, Zeng H, Bray F, et al. Cancer statistics in China, 2015. CA Cancer J Clin 2016;66:115–32.
2. Voltaggio L, Cimino-Mathews A, Bishop JA, Argani P, Cuda JD, Epstein JI, et al. Current concepts in the diagnosis and pathobiology of intraepithelial neoplasia: a review by organ system. CA Cancer J Clin 2016;66:408–36.
3. Pan Y, Volkmer JP, Mach KE, Rouse RV, Liu JJ, Sahoo D, et al. Endoscopic molecular imaging of human bladder cancer using a CD47 antibody. Sci Transl Med 2014;6:260ra148.
4. Stamatiou K, Papadoliopoulos I, Dahanis S, Zafiropoulos G, Polizois K. The accuracy of ultrasonography in the diagnosis of superficial bladder tumors in patients presenting with hematuria. Ann Saudi Med 2009;29:134–7.
5. Frantzi M, van Kessel KE, Zwarthoff EC, Marquez M, Rava M, Malats N, et al. Development and validation of urine-based peptide biomarker panels for detecting bladder cancer in a multi-center study. Clin Cancer Res 2016;22:4077–86.
6. Babjuk M, Burger M, Zigeuner R, Shariat SF, van Rhijn BW, Compérat E. EAU guidelines on non-muscle-invasive urothelial carcinoma of the bladder: update 2013. Eur Urol 2013;64:639–53.
7. Wang LV, Hu S. Photoacoustic tomography: *in vivo* imaging from organelles to organs. Science 2012;335:1458–62.
8. Lerner SP, Goh A. Novel endoscopic diagnosis for bladder cancer. Cancer 2015;121:169–78.
9. Witjes JA, Redorta JP, Jacqmin D, Sofras F, Malmström PU, Riedl C, et al. Hexaminolevulinate-guided fluorescence cystoscopy in the diagnosis and follow-up of patients with non-muscle-invasive bladder cancer: review of the evidence and recommendations. Eur Urol 2010;57:607–14.
10. Stenzl A, Penkoff H, Dajc-Sommerer E, Zumbraegel A, Hoeltl L, Scholz M. Detection and clinical outcome of urinary bladder cancer with 5-aminolevulinic acid-induced fluorescence cystoscopy: a multicenter randomized, double-blind, placebo-controlled trial. Cancer 2011;117:938–47.
11. James ML, Gambhir SS. A molecular imaging primer: modalities, imaging agents, and applications. Physiol Rev 2012;92:897.
12. Sato AK, Viswanathan M, Kent RB, Wood CR. Therapeutic peptides: technological advances driving peptides into development. Curr Opin Biotechnol 2006;17:638–42.
13. Brown KC. Peptidic tumor targeting agents: the road from phage display peptide selections to clinical applications. Curr Pharm Des 2010;16:1040–54.
14. Chen K, Sun X, Niu G, Ma Y, Yap LP, Hui X, et al. Evaluation of 64Cu labeled GX1: a phage display peptide probe for PET imaging of tumor vasculature. Mol Imaging Biol 2012;14:96–105.
15. Larimer BM, Deutscher SL. Development of a peptide by phage display for SPECT imaging of resistance-susceptible breast cancer. Am J Nucl Med Mol Imaging 2014;4:435–47.
16. Yang X, Fan Z, Luo J, Pang J, Yan S, Fang L, et al. A new non-muscle-invasive bladder tumor-homing peptide identified by phage display in vivo. Oncol Rep 2016;36:79–89.
17. Soendergaard M, Newtonnorthup JR, Deutscher SL. In vivo phage display selection of an ovarian cancer targeting peptide for SPECT/CT imaging. Am J Nucl Med Mol Imaging 2014;4:561–70.
18. Larimer BM, Phelan N, Wehrenberg-Klee E, Mahmood U. Phage display selection, in vitro characterization, and correlative PET imaging of a novel HER3 peptide. Mol Imaging Bio 2018;20:300–8.
19. Madajewski B, Judy BF, Mouchli A, Kapoor V, Holt D, Wang MD, et al. Intraoperative near-infrared imaging of surgical wounds after tumor resections can detect residual disease. Clin Cancer Res 2012;18:5741–51.
20. Lee SM, Lee EJ, Hong HY, Kwon MK, Kwon TH, Choi JY, et al. Targeting bladder tumor cells in vivo and in the urine with a peptide identified by phage display. Mol Cancer Res 2007;5:11–9.
21. Zhang H, Aina OH, Lam KS, De VWR, Evans C, Henderson P, et al. Identification of a bladder cancer-specific ligand using a combinatorial chemistry approach. Urol Oncol 2012;30:635–45.

Published OnlineFirst August 6, 2018; DOI: 10.1158/1535-7163.MCT-18-0212

22. Horton DA, Bourne GT, Smythe ML. Exploring privileged structures: the combinatorial synthesis of cyclic peptides. Cheminform 2002;5: 289–304.
23. Bosschieter J, Nieuwenhuijzen JA, Van GT, Vis AN, Witte B, Newling D, et al. Value of an immediate intravesical instillation of mitomycin C in patients with non-muscle-invasive bladder cancer: a prospective multicentre randomised study in 2243 patients. Eur Urol 2018;73: 226–32.
24. Watanabe T, Shinohara N, Sazawa A, Harabayashi T, Ogiso Y, Koyanagi T, et al. An improved intravesical model using human bladder cancer cell lines to optimize gene and other therapies. Cancer Gene Ther 2000;7:1575–80.
25. Nicolau C, Bunesch L, Sebastia C, Salvador R. Diagnosis of bladder cancer: contrast-enhanced ultrasound. Abdom Imaging 2010;35: 494–503.
26. Luke GP, Hannah AS, Emelianov SY. Super-resolution ultrasound imaging *in vivo* with transient laser-activated nanodroplets. Nano Lett 2016;16: 2556–9.
27. Liu C, Gong X, Lin R, Feng L, Chen J, Wang Z, et al. Advances in imaging techniques and genetically encoded probes for photoacoustic imaging. Theranostics 2016;6:2414–30.
28. Zerda ADL, Liu Z, Bodapati S, Teed R, Vaithilingam S, Khuri-Yakub BT, et al. Ultrahigh sensitivity carbon nanotube agents for photoacoustic molecular imaging in living mice. Nano Lett 2010;10:2168–72.
29. Liu JJ, Droller MJ, Liao JC. New optical imaging technologies for bladder cancer: considerations and perspectives. J Urol 2012;188:361–8.
30. Lin T, Li Y, Liu Q, Chen JL, Zhang H, Lac D, et al. Novel theranostic nanoporphyrins for photodynamic diagnosis and trimodal therapy for bladder cancer. Biomaterials 2016;104:339–51.
31. Witjes JA, Babjuk M, Gontero P, Jacqmin D, Karl A, Kruck S, et al. Clinical and cost effectiveness of hexaminolevulinate-guided blue-light cystoscopy: evidence review and updated expert recommendations. Eur Urol 2014;66: 863–71.
32. Ye Z, Hu J, Song X, Li F, Zhao X, Chen S, et al. A comparison of NBI and WLI cystoscopy in detecting non-muscle-invasive bladder cancer: a prospective, randomized and multi-center study. Sci Rep 2015;5:10905.

Published OnlineFirst August 6, 2018; DOI: 10.1158/1535-7163.MCT-18-0212

Molecular Cancer Therapeutics

Phage Display-Derived Peptide-Based Dual-Modality Imaging Probe for Bladder Cancer Diagnosis and Resection Postinstillation: A Preclinical Study

Li Peng, Wenting Shang, Pengyu Guo, et al.

Mol Cancer Ther 2018;17:2100-2111. Published OnlineFirst August 6, 2018.